SLAC-PUB-630
July 1969
(EXPI) and (ACC)

THE STANFORD POSITRON-ELECTRON ASYMMETRIC RINGS (SPEAR)*

SLAC Storage Ring Group

presented by

B. Richter

Stanford Linear Accelerator Center, Stanford University, Stanford, California

I. Introduction

The SLAC storage ring group has for many years been seeking authorization to begin construction of a high luminosity, 3-GeV, electron-positron storage ring. Although this project has had strong support from the scientific community, it has not been approved for reasons primarily having to do with cost and availability of funds.

In January of this year we began conducting an intensive review of alternative storage ring designs with the objective of drastically reducing the cost of the project while maintaining the ability to do a great deal of the most interesting physics outlined in our 1966 proposal, particularly that part involving strongly interacting particles. This review was conducted in the light of recent experiences with beam instabilities at both Frascati and Orsay, and the result is SPEAR (Stanford Positron-Electron Asymmetric Rings), a new two-stage proposal for a double ring with a large horizontal crossing angle at the interaction regions.

Our choice of energy and circulating current involves a compromise between accessible physics and costs. Our compromise has the following rough parameters for each beam (more precise numbers are given later).

	STAGE I	STAGE II
E_{Max} (GeV)	2	3
I_{Max} (amps)	$0.5\times(2/E)^4$	$1.0\times(3/E)^4$
L_{Max} ($cm^{-1}sec^{-1}$)	$10^{32}\times(2/E)^3$	$3\times10^{32}\times(3/E)^3$
Crossing Angle (deg.)	10.5	10.5

With an energy of 2 GeV for each beam in Stage I we are above threshold for pair production of all of the long-lived mesons and baryons and most of the meson and baryon resonances. To see them, however, it is likely that we shall need a very large luminosity. In choosing the luminosity for Stage I, we assumed that the cross section for proton-antiproton pair production would be typical of the cross section for producing pairs of strongly interacting particles, and required a reasonable counting rate for a fairly pessimistic estimate of the form factor.[1] With a form factor[2] of

$$G_E = G_M = \left(1 + \frac{|q^2|}{0.71}\right)^{-2} \qquad (1)$$

and the design luminosity, we will get a counting rate of a few per hour for $P\bar{P}$ at 1.5 GeV.

II. Choice of Interaction Region Geometry

The most novel feature of the design is the 10^o horizontal crossing angle which is unusual in electron storage ring design although it is the approach used in the CERN ISR project and in most other proton storage ring designs. The layout of the new rings is shown schematically in Fig. 1. Each ring consists of 2 matched small β inserts connected by arcs of unequal length, the longer arc containing six cells and the shorter arc five cells. The two rings are interlaced to make two interaction regions with the beams making an angle of about 10 degrees. Many nominally three-meter straight sections are available for injection, rf, nonlinear correcting magnets, beam sensing and feedback elements, etc.

Since this design is so different from our previous proposal, I will describe briefly the rationale for our choice. The double ring with horizontal crossing evolved during our design review from consideration of how best to achieve high luminosity and beam stability. Currently operating storage rings have been plagued with coherent single-beam as well as with the familiar incoherent two-beam instability. We concluded that all these effects could best be controlled if the beams were widely separated and thus would be non-interacting, and could be sensed and acted on independently. At first glance, this approach which requires separate guide fields for each ring, would seem to go counter to our objective of reducing costs. As we shall see, this is not so.

The limitation on current density allowable at the interaction region is conventionally expressed in terms of a limitation on the vertical tune shift that a particle in one beam would experience in passing through the other beam.[3] This is given by

$$\Delta\nu_V = \frac{a_1 I \beta_V}{fEA} \leq \Delta\nu_0 = 0.025 \ , \qquad (2)$$

where a_1 is a constant, I is the beam current, β_V is taken at the interaction point, f is the orbit frequency, E the beam energy, and A the effective beam area. The luminosity is given by

$$L = a_2 \frac{I^2}{fA} \leq L_{Max} \qquad (3a)$$

$$L_{Max} \propto \Delta\nu_0^2 \ A \ E^2/\beta_V^2 \ . \qquad (3b)$$

The maximum luminosity which can be reached in a given guide field depends only on the effective area of the beams, assuming that the limit on $\Delta\nu_V$ can be reached and that an analogous limit on $\Delta\nu_H$ is not violated.

*Work supported by U.S. Atomic Energy Commission.

To be presented at 7th Int.Conf. on High Energy Acc., Yerevan, Armenia, USSR, Aug. 27-Sept. 2, 1969

For Gaussian beams the effective area is given by

$$A \approx 2\pi k(\sigma_V + \sigma_\ell \delta_V)(\sigma_H + \sigma_\ell \delta_H),$$

where k is the number of bunches in the ring, σ_H, σ_V, and σ_ℓ are respectively the horizontal, vertical, and longitudinal standard deviations of the particle distributions within a bunch, and δ_V and δ_H are respectively the vertical and horizontal crossing angles. For the very large luminosities we hope to reach at beam energies lower than the maximum, A must be larger than the "natural" cross-sectional area given by $\delta_V = \delta_H = 0$, σ_H determined by the quantum fluctuation in synchrotron radiation, and σ_V determined by a reasonable horizontal-vertical coupling.

A can be increased either by introducing a crossing angle or by artificially increasing the size of the beam. However, an incoherent increase in the beam size has not proved easy to achieve, and also requires an increase in the aperture of the ring with corresponding increases in the costs. In a single ring the aperture is further increased by the requirement imposed by the condition of Eq. (2) on two-beam interactions outside of the low β "target" area. Since β_V is much larger in the normal part of the machine than in the target area, the beams must be separated by several times their height, requiring a further increase in aperture both for the beam separation and for the high field electrodes required to make the separation. These extra aperture requirements result in comparable magnet and vacuum chamber costs for a single or a double ring system.

A double ring design also makes the problem of feedback control of single-beam coherent instabilities much simpler than in the single ring. Both the tune and the synchrotron oscillation frequency of each beam are under independent control in the double ring. Injection is somewhat simpler into a double ring since there is no perturbation of the newly injected beam by fields associated with the large current of the other beam.

All the above factors make us prefer a double ring design. Three further factors make us prefer the large horizontal crossing angle with widely separated rings to the smaller vertical crossing angle of the vertically separated double ring design of the DESY type.[4] (The DESY group was the first to suggest separate rings for high energy $e^+ - e^-$ colliding beams.) Firstly, the small β insertion is much simpler in the horizontal crossing case. No strong electric fields, septum magnets, or vertical bends are required to separate the beams and lead them into the normal guide field, and the zero dispersion insertion design developed for our previous proposal is directly applicable.[5]

Secondly, the beams are completely separated at the strong quadrupoles closest to the interaction region where β is very large. This decreases the aperture required in these quads and assures that there are no nonlinear interactions of the two beams which might cause problems.

Thirdly, there are advantages to a class of physics experiments in the large crossing angle which come from the finite velocity of the center-of-mass of the colliding beams. For example, the proton-antiproton final state can be separated from other two-body final states solely on the basis of the angle between the two outgoing particles, and this separation is preserved in the presence of the first-order radiation correction. It is therefore possible to study this reaction without a magnetic field detector.

III. Lattice and Luminosity

The SPEAR magnet lattice is based on the structure developed for our 1966 proposal. Figure 2 shows the structure, β functions, and momentum vector for a standard cell in the long arc. The short arc must have a smaller average radius of curvature than the long arc, in order to close the ring. We have chosen to accomplish this by keeping the bending magnet and quadrupole fields and lengths identical in the two regions and shortening the three-meter straight section in the standard cell by roughly 1/2 meter to make the cells of the short arc. Since the first and second derivatives of the β function are very small at the center of the cell straight section, this makes a negligible perturbation on the transfer matrix of the cell.

The small β insertion is also nearly identical to our old design. Its properties are shown in Fig. 3. At the center of the interaction region β_V is nominally five cm and is continuously adjustable up to a value of a few meters by adjusting the currents in Q_1, Q_2, and Q_3. The momentum vector η has been made zero in the central region of the insert in order to allow this variation in β without spoiling the momentum match to the rest of the ring.

The normal tune of each ring is around $\nu_H = 5.2$, $\nu_V = 5.1$. These can be varied from roughly 4.5 to 5.7 with little difficulty. To maintain a perfect momentum match over this region, the quadrupole QF_1 in the interaction must be physically moved from its nominal position. Over a region of tune of about ± 1/4, the match is satisfactory without varying the position of QF_1.

Figure 4 shows the interaction region. The two rings cross at an angle of 10.5° and, after the 2.5-meter drift distance from the interaction point to the beginning of Q_3, the beam center lines are separated by 1/2 meter, allowing the use of independent quadrupoles in the two rings. Vertical clearance in the interaction region housing for detection apparatus is ± 3.5 meters.

The design luminosity of SPEAR is given in Fig. 5, where we have assumed one beam-beam collision per turn. The curve labeled I is appropriate to the Stage I design with 60 kW of rf power available for each beam and the curve labeled II is that appropriate to 550 kW of power for each beam in Stage II. The parts of the curves with negative slope correspond to rf-power-limited operation where $\Delta\nu$ is made equal to $\Delta\nu_{Max}$ by adjusting the effective value of the beam area. We assume that the minimum value of the beam height in the normal part of the ring will be set by residual horizontal-vertical couplings and will be about 1/10 of the beam width. By varying the number of filled bunches from 1 to 36 and by varying the horizontal-vertical coupling the effective beam area can be made to cover a range of 360 to 1. In Stage I the luminosity is roughly 10^{32} cm^{-2} sec^{-1} at 2 GeV.

As the energy of the circulating beams is decreased, the effective area required to reach the maximum value of $\Delta\nu$ increases and eventually reaches a limit set by the aperture of the vacuum chamber. At this point the luminosity is a maximum, and for energies below this critical energy the effective area must remain fixed and $\Delta\nu$ can no longer be made equal to the maximum value. The luminosity then drops as the E^3. For Stage I of SPEAR this maximum luminosity is about 1.5×10^{33} cm^{-2} sec^{-1} and occurs at an energy of about 0.8 GeV.

The very large luminosities attainable at low energy in SPEAR require very large circulating beam currents, up to 20 amps at the critical energy in Stage I. It is possible that at these very large values of circulating current some new beam instability will arise to plague us. I have therefore indicated on Fig. 5 by the dashed curves the luminosity attainable in the event that the maximum circulating beam current is limited.

IV. Design Details

In this section I will briefly describe some of the design features of the rings, which may be of interest. Since the design has not yet been frozen, some of the final parameters may be somewhat different from those given here.

A. Magnets. The magnets are of conventional design. Each quadrupole will be fabricated of four identical quadrants made from 1/8-inch-thick steel laminations. The bending magnets are conventional H magnets. They are not laminated and will be made from rolled steel plate. All magnet coils will be made of aluminum which we find to be considerably cheaper than copper coils. Each magnet will be provided with an auxiliary coil capable of handling 1/4% of the ampere turns of the main coil. These coils can be used to eliminate the closed-orbit deviation by compensating for field errors and small quadrupole misalignments. All magnets are designed to operate at fields corresponding to 3-GeV beams, but in Stage I power will only be supplied to run the magnets to 2 GeV.

B. RF. The rf system will run at a frequency of about 50 Mc on the 36th harmonic of the orbit frequency. There will be one rf cavity for each ring. Power available in Stage I is to be 60 kW for each ring. The energy loss per turn in synchrotron radiation at 2 GeV is 110 kV and the maximum rf voltage available is 200 kV, giving a quantum fluctuation lifetime of $> 10^5$ sec at 2 GeV. At the injection energy of 1-1/2 GeV, the momentum acceptance is $\pm$ 1/2%.

C. Injection. We plan to inject into the storage ring at energies ≤ 1.5 GeV. Since SPEAR will be located at the end of the 20-GeV linac rather than at the two-thirds point, as in our 1966 proposal, the positron intensity is expected to be lower, because of the longer distance over which the low-energy positron beam must be transmitted. With this lower energy injection the radiation damping times are also increased and hence the injection frequency is decreased. The injection system is a standard beam-bump-and-septum design and we plan to inject twice per damping time. Under these conditions we expect to get an injection rate of about 2 circulating amperes per minute at 1-1/2 GeV.

D. Vacuum. The vacuum chamber will be fabricated of aluminum extruded in the proper cross section, including the water passage to carry off heat generated by the absorption of synchrotron radiation. We chose aluminum over the more conventional stainless steel because an aluminum chamber is easier to fabricate, has a lower gas desorption coefficient and a lower x-ray reflection coefficient. The inside surface of the vacuum chamber where synchrotron radiation will strike will be corrugated to further reduce the gas desorption rate.

We plan to use ion pumps on the ring but the exact configuration is not yet settled. We are experimenting with distributed ion pumps which use the relatively low-quality magnetic field of the bending magnets near the pole edge for the magnetic field required on the pumps. The components of one of these pumps are shown in Fig. 6. The pump is made from pieces of stainless steel tubing spot-welded together, and the necessary insulators to support this structure at high voltage ($\sim$ 5 kV) between two 0.080"-thick titanium plates. The results to date are extremely promising. With ion pump cells 1/2 inch in diameter we have achieved pumping speeds of 450 ℓ/sec/m of pump for nitrogen or carbon monoxide with 1200, 45, and 5 ℓ/sec/m for hydrogen, helium, and argon, respectively. This pumping speed is nearly independent of magnetic field down to fields of about 1.8 kG which corresponds in our design to 0.75-GeV circulating beams. If this system works out well, we will use 1 m of this distributed pump in each bending magnet and use relatively small conventional ion pumps in each cell straight section to hold the pressure down when the bending magnets are off and no beam is circulating in the ring.

E. Assembly. We plan to preassemble the components of the ring into modules as shown in Fig. 7 before installation in the storage ring housing. Each module is composed of a 30-ft concrete support girder, on which 2 bending magnets and 3 quadrupoles are typically mounted. These are elements of a normal cell less the cell straight section. The magnets will be aligned with respect to the girder, the vacuum chamber installed and leak-checked, and all power, water, and control cabling installed. Installation of this module in the ring requires the alignment of the concrete support girder and the connection of one water pipe, three dc power cables, and one multiconductor control cable.

V. Status

We have requested authorization for construction of Stage I in the fiscal year beginning July, 1970, and with specific encouragement from the Congressional Joint Committee on Atomic Energy and from the AEC, have begun an intensive research and development program this year. Our goal is to move rapidly from research and development to construction, and to complete construction within two years of its start. The cost of this project is expected to be about $9 million.

References

1. See, for example, Chan et al., Phys. Rev. 141, 1298 (1966).

2. The usual dipole form factors used in the space-like momentum transfer region are $G_E = G_{M/\mu} = (1 + q^2/0.71)^{-2}$. However there is a threshold constraint in pair production at $q^2 = 4M^2$ which forces $G_E = G_M$.

3. E. D. Courant, BNL Internal Report No. AADD-69, (March 1965).

4. DESY Storage Ring Proposal (1967).

5. P. L. Morton and J. R. Rees, IEEE Trans. Nucl. Sci. NS-14, 630 (1967).

FIGURE CAPTIONS

FIG. 1--Schematic of the double ring.

FIG. 2--Magnet lattice, β functions (left scale) and the equilibrium orbit for off-momentum particles (η, right scale) in a standard cell.

FIG. 3--Magnet lattice, β functions (left scale) and the equilibrium orbit for off-momentum particles (η, right scale) in the low β orbit.

FIG. 4--The interaction region. The pit below the beam crossing gives 3.5-meter vertical clearance for detection apparatus. The separation between the closest quadrupoles is 5 meters.

FIG. 5--Luminosity versus energy for Stage I and Stage II (solid curves). The dashed curves indicate the maximum luminosity which can be achieved with a given circulatory current.

FIG. 6--Components of the 500-liter-per-second distributed ion pump.

FIG. 7--Schematic of a preassembled ring module.

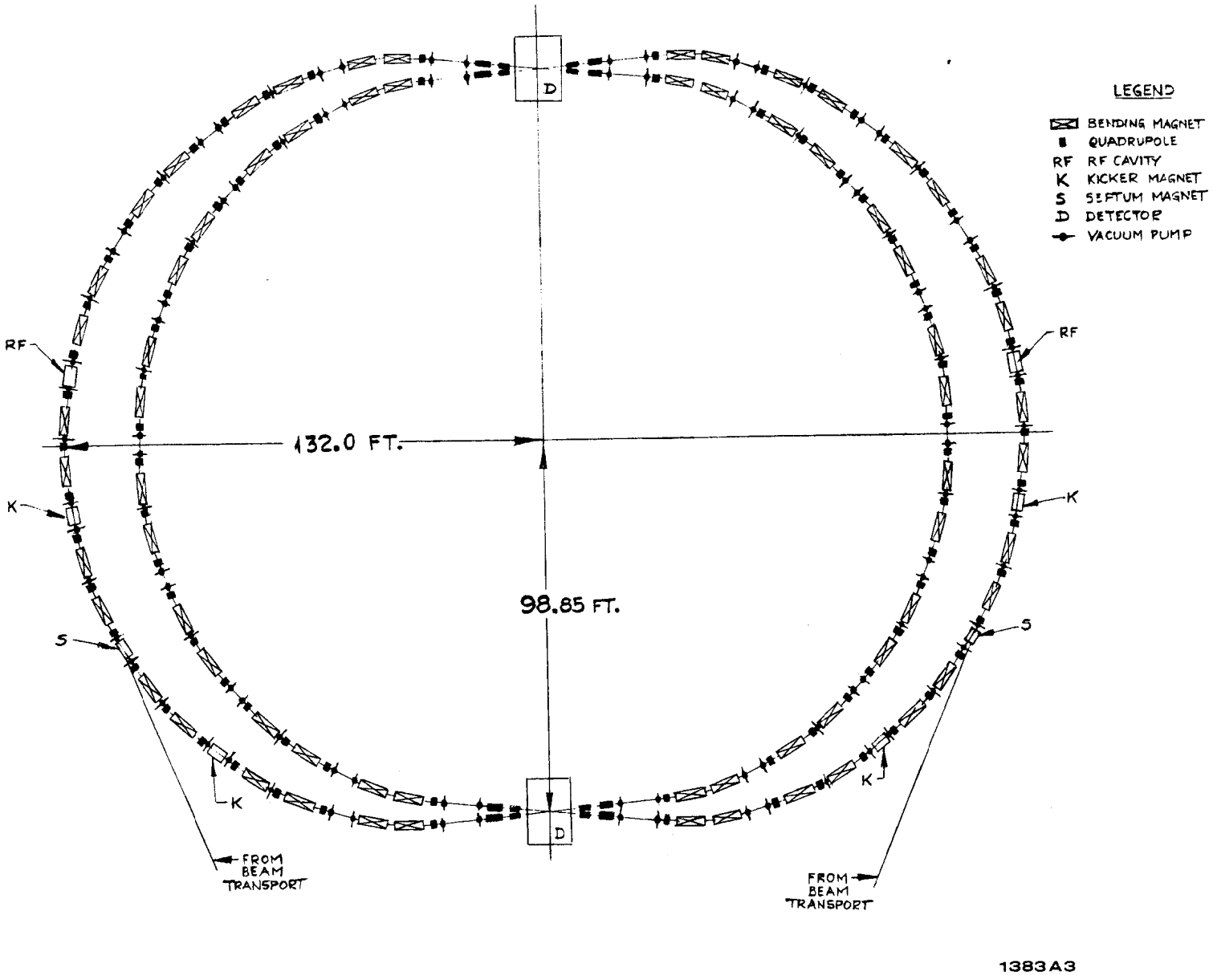
LEGEND
BENDING MAGNET
QUADRUPOLE
RF RF CAVITY
K KICKER MAGNET
S SEPTUM MAGNET
D DETECTOR
VACUUM PUMP
D
RF
RF
132.0 FT.
K
K
98.85 FT.
S
S
K
K
D
FROM BEAM TRANSPORT
FROM BEAM TRANSPORT
1383A3

Fig. 1

Component	Type of Component	Approximate Field or Gradients at 3 GeV
QD	Defocusing Quadrupole	-0.6 kG/cm
BB	Bending Magnet (n = 0)	7.5 kG
QF	Focusing Quadrupole	0.3 kG/cm

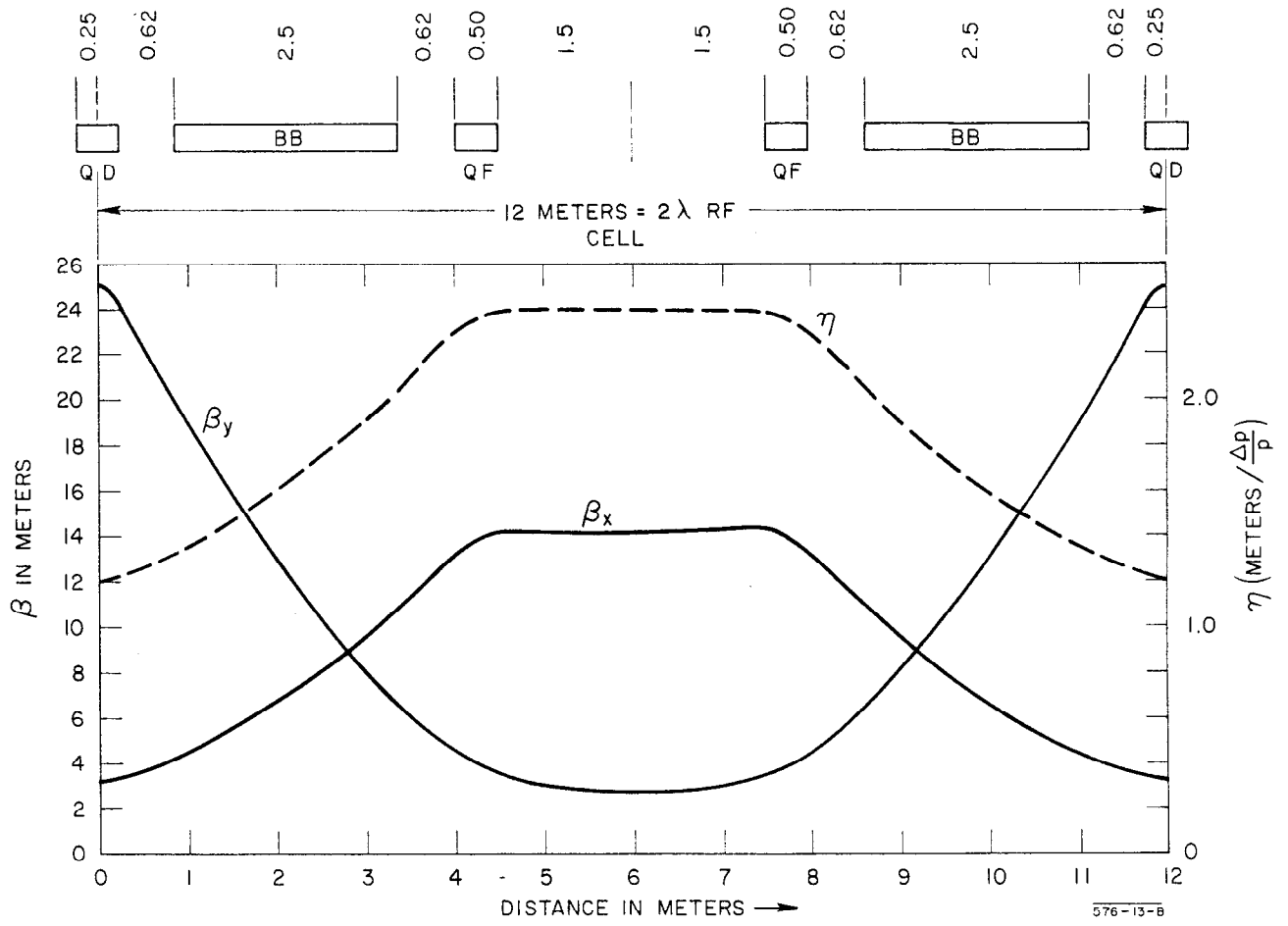

Fig. 2

Component	Type of Component	Approximate Field or Gradients at 3 GeV
QD	Defocusing Quadrupole	- 0.6 kG/cm
BB	Bending Magnet (n=0)	7.5 kG
QF1	Focusing Quadrupole	0.7 kG/cm
Q1	Defocusing Quadrupole	- 0.03 kG/cm
Q2	Focusing Quadrupole	0.4 kG/cm
Q3	Defocusing Quadrupole	- 0.7 kG/cm

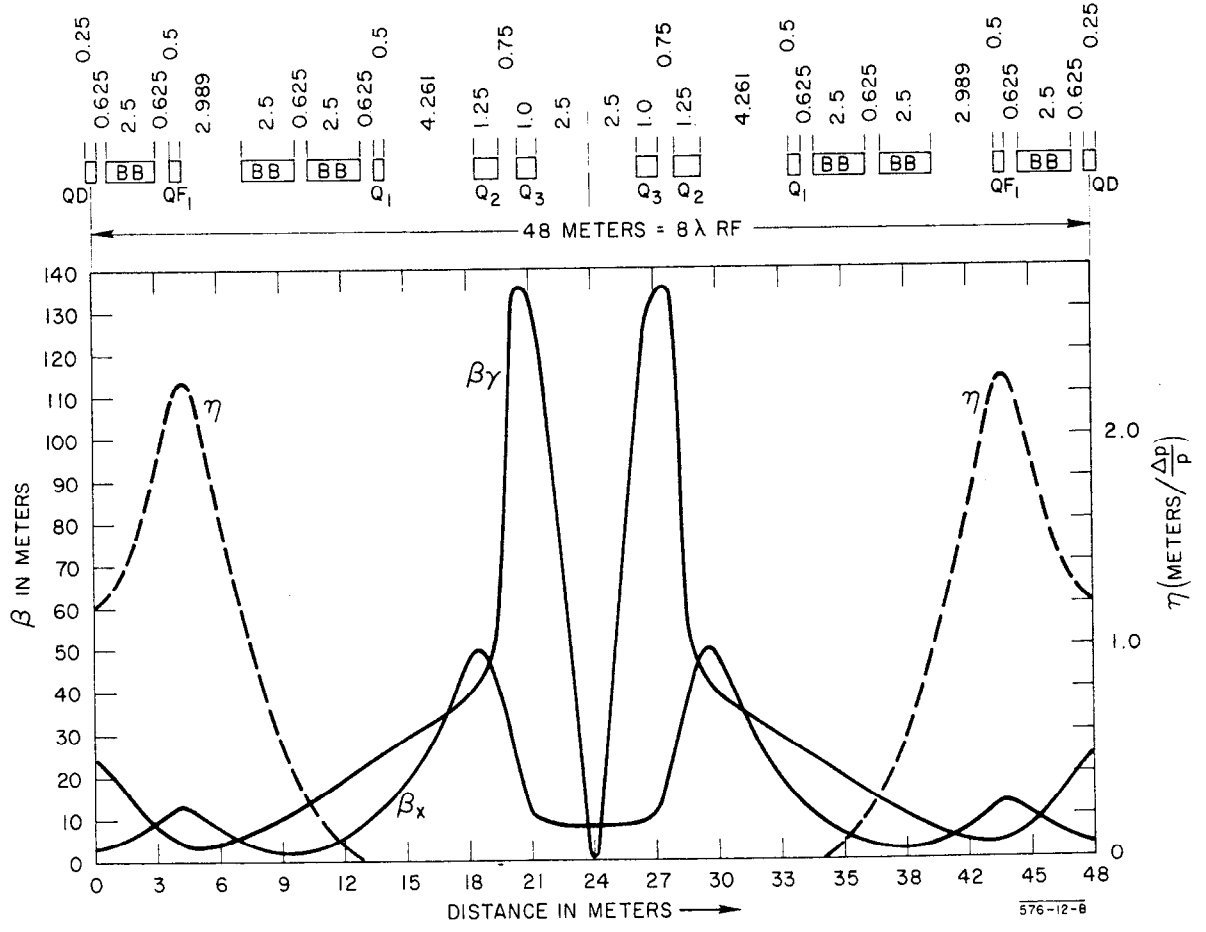

Fig. 3

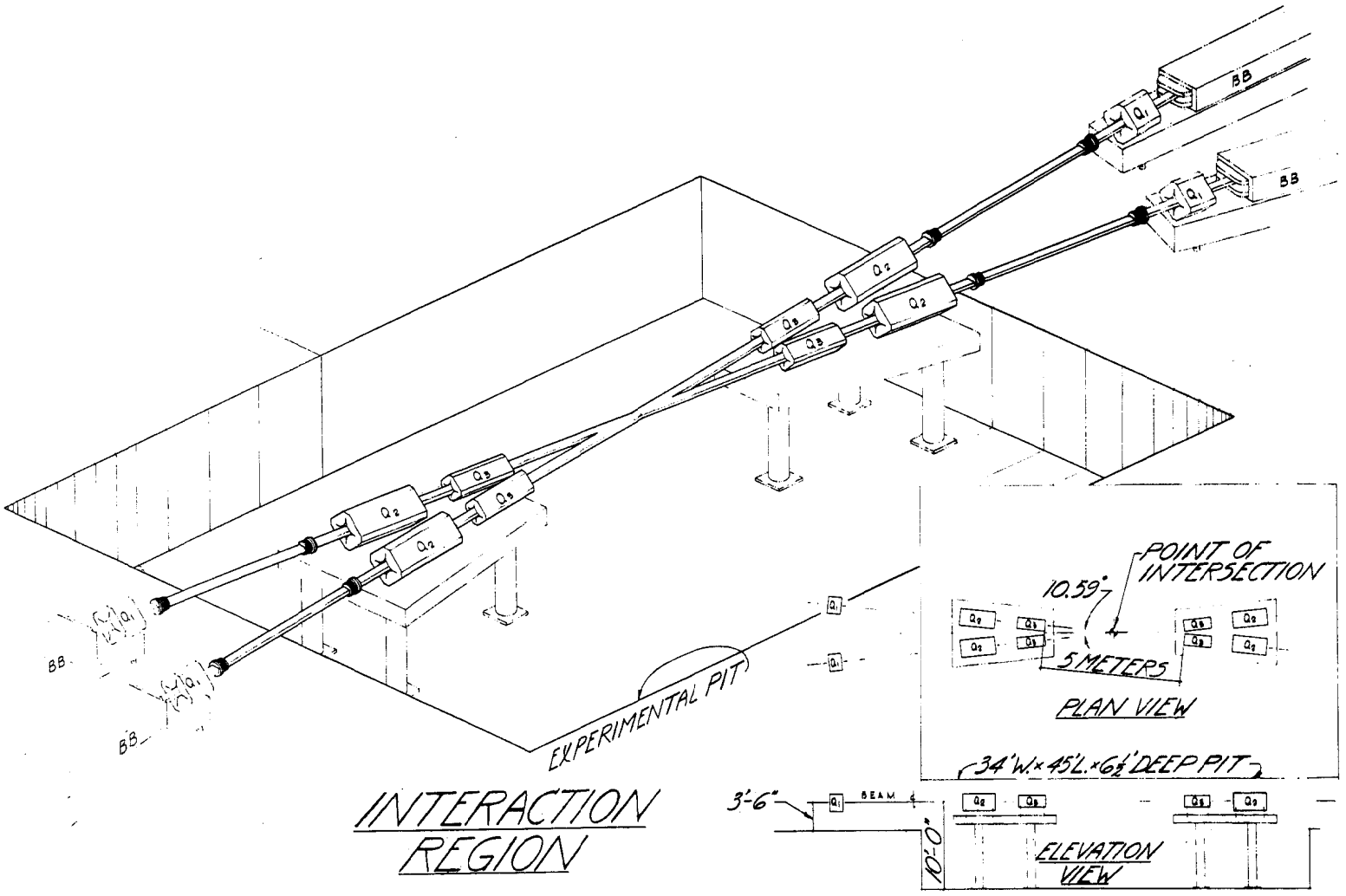
BB
BB
BB
EXPERIMENTAL PIT
INTERACTION REGION
POINT OF INTERSECTION
10.59°
5 METERS
PLAN VIEW
34'W.×45'L.×6½'DEEP PIT
3'-6"
BEAM
10'-0"
ELEVATION VIEW

1383E4

Fig. 4

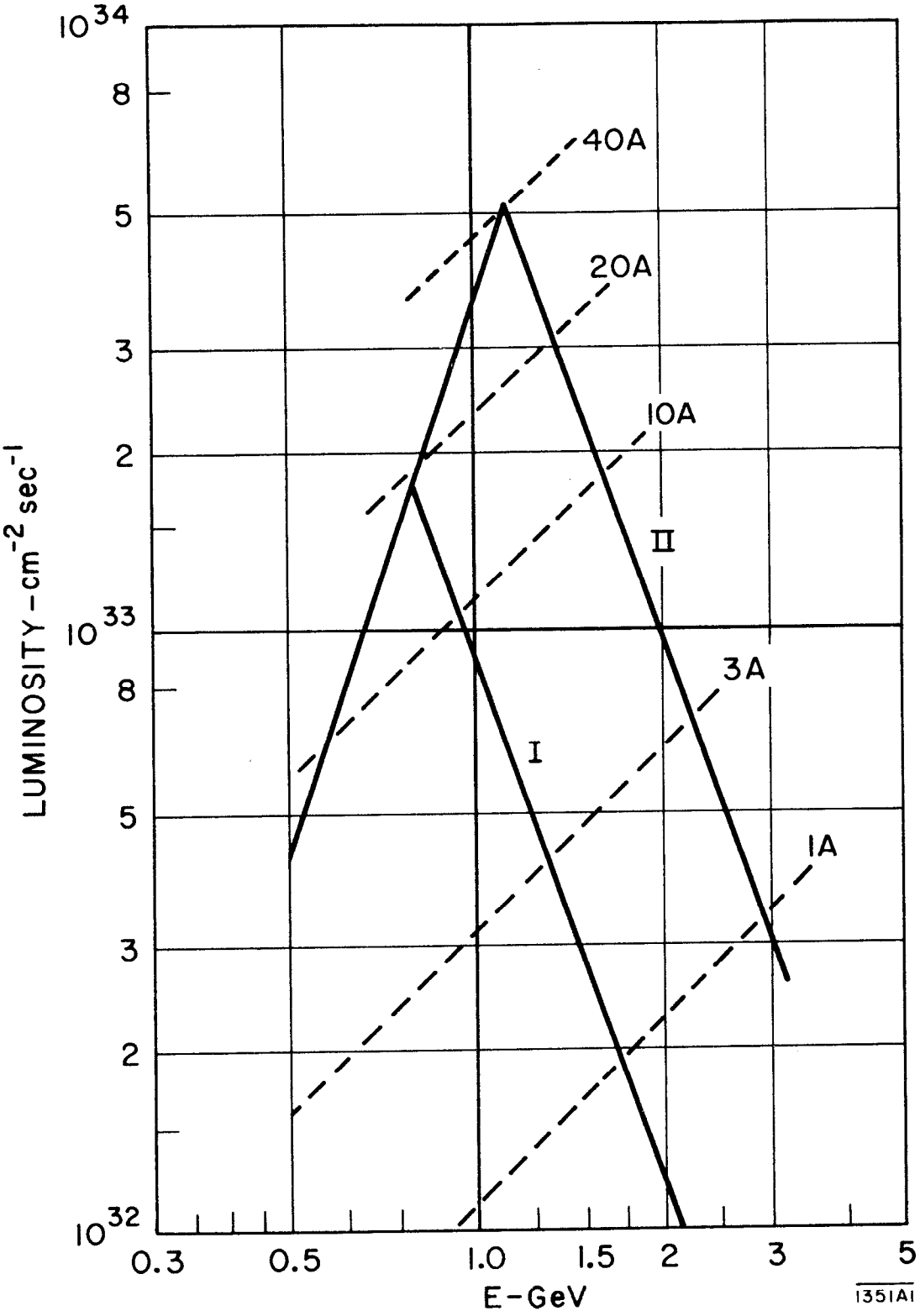
LUMINOSITY - cm^{-2} sec^{-1}
10^{34}
8
5
3
2
10^{33}
8
5
3
2
10^{32}
40A
20A
10A
3A
1A
II
I
0.3
0.5
1.0
1.5
2
3
5
E-GeV
1351A1

Fig. 5

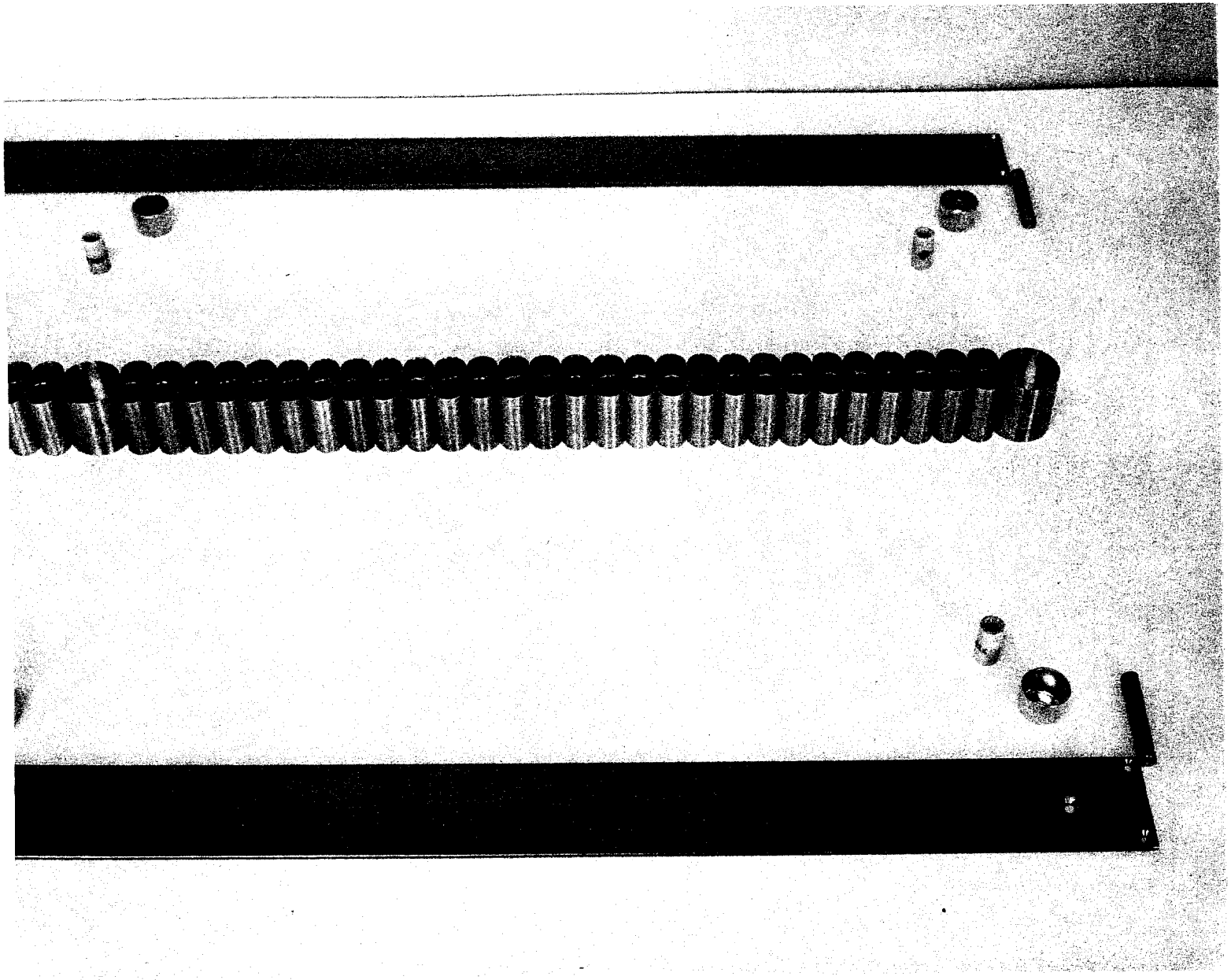

1383A6

Fig. 6

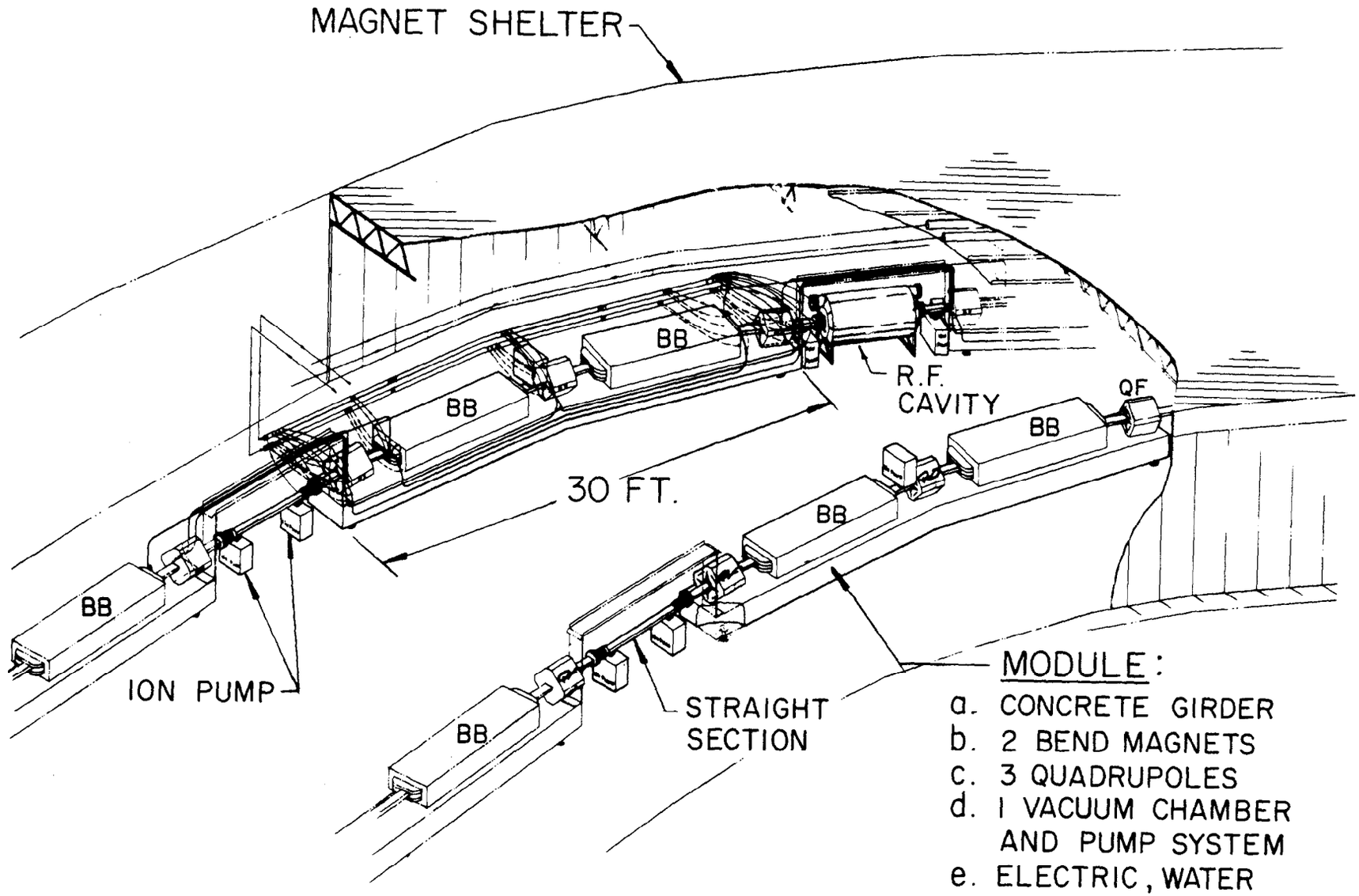
MAGNET SHELTER
BB
BB
R.F.
CAVITY
QF
BB
30 FT.
BB
BB
ION PUMP
STRAIGHT
SECTION
MODULE:
a. CONCRETE GIRDER
b. 2 BEND MAGNETS
c. 3 QUADRUPOLES
d. 1 VACUUM CHAMBER
AND PUMP SYSTEM
e. ELECTRIC, WATER
AND I & C SERVICES
SLAC STORAGE RINGS
1383A7

Fig. 7